Deep learning for channel tracking in IRS-assisted UAV communication systems

Deep Learning for Channel Tracking in IRS-Assisted UAV Communication Systems

Jiadong Yu, Xiaolan Liu, Yue Gao, Chiya Zhang, Wei Zhang

***Abstract*—To boost the performance of wireless communication networks, unmanned aerial vehicles (UAVs) aided communications have drawn dramatically attention due to their flexibility in establishing the line of sight (LoS) communications. However, with the blockage in the complex urban environment, and due to the movement of UAVs and mobile users, the directional paths can be occasionally blocked by trees and high-rise buildings. Intelligent reflection surfaces (IRSs) that can reflect signals to generate virtual LoS paths are capable of providing stable communications and serving wider coverage. This is the first paper that exploits a three-dimensional geometry dynamic channel model in IRS-assisted UAV-enabled communication system. Moreover, we develop a novel deep learning based channel tracking algorithm consisting of two modules: channel pre-estimation and channel tracking. A deep neural network with off-line training is designed for denoising in the pre-estimation module. Moreover, for channel tracking, a stacked bi-directional long short term memory (Stacked Bi-LSTM) is developed based on a framework that can trace back historical time sequence together with bidirectional structure over multiple stacked layers. Simulations have shown that the proposed channel tracking algorithm requires fewer epochs to convergence compared to benchmark algorithms. It also demonstrates that the proposed algorithm is superior to different benchmarks with small pilot overheads and comparable computation complexity.**

***Index Terms*—Channel Tracking, Deep Learning (DL), Intelligent Reflection Surfaces (IRS), Long Short Term Memory (LSTM), Unmanned Aerial Vehicles (UAV).**

I. Introduction

Unmanned aerial vehicles (UAVs) acting as aerial base stations can provide a solution on serving wider coverage, supporting reliable connections, and providing energy efficient communications [1], [2]. The flexibility of UAVs has led to plenty of applications such as security surveillance, real-time monitoring, rescue, and emergency communications [3]. Although UAV-aided systems are considered as promising techniques for future wireless communications for smart city, the complex urban environment poses potential blockage problem on LoS links between navigation UAVs and ground users [4]. IRSs that can construct virtual LoS paths to enhance the quality and coverage of wireless propagation has become an invaluable solution on overcoming signal pathloss and on securing communications [5], [6]. This is because that the low-cost IRS can intelligently adjust its phase shifts to steer signal power towards targeted directions and reduce information leakage. Thus, to address the blockage problem in UAV-aided system, intelligent reflection surfaces (IRSs) can be installed to assist the UAV to offer ubiquitous communication services [4], [7]–[9]. Additionally, deploying IRSs in the UAV-aided system can further help with the time- and energy- consuming problem caused by UAV navigation when some users are far away [7]. Therefore, with the appealing advantages of UAV and IRS, deploying both of them in the wireless system can dramatically boost the communication performance.

Moreover, to achieve high quality communications, it is indispensable to acquire accurate channel state information (CSI) for effective transmissions. Compared to the CSI estimation in the conventional communication systems, channel tracking in IRS-assisted UAV systems are more challenging in a time-varying environment with small overheads. Since IRS is unable to perform signal processing, the large number of reflecting elements of IRS, and the mobility of UAV and users all leads to high complexity.

A. Related Work

For future wireless communications, the widely studied challenge is to achieve ultra-reliable and high-capacity wireless communications in a time-varying environment. A lot of efforts have been focused on designing efficient coding and modulation schemes and on implementing power and beamforming control. However, these studies ignore the wireless channel between the communication ends. Thus, emerging technologies such as UAV-assisted and IRS-aided communications have received extensive attention in recent years [10].

Compared to the terrestrial base stations, the UAV-based aerial base stations' advantage is the adjustable altitude and mobility. This flexibility enables UAVs to play a vital role in wireless communications. Particularly, UAVs can assit the

J. Yu is with the Internet of Things Thrust, The Hong Kong University of Science and Technology, Guangzhou 511400, China (email: jiadongyu@ust.hk).

X. Liu is with the Institute for Digital Technologies, Loughborough University London, London E20 3BS, UK (email: xiaolan.liu@lboro.ac.uk).

Y. Gao (corresponding author) is with the School of Computer Science, Fudan University, Shanghai 200438, China email: gao_yue@fudan.edu.cn).

Chiya Zhang is with the School of Electronic and Information Engineering, Harbin Institute of Technology, Shenzhen, China. He is also with Peng Cheng Laboratory(PCL), Shenzhen 518055, China (zhangchiya@hit.edu.cn).

W. Zhang is with the School of Electrical Engineering and Telecommunications, University of New South Wales, Sydney, NSW 2052, Australia (e-mail: wzhang@ee.unsw.edu.au).

This work was supported by National Key R&D Program of China under Grant 2020YFA0711400, Key Area Research and Development Program of Guangdong Province under grant No. 2020B0101110003, Shenzhen Science Innovation Fund under Grant JCYJ20180507182451820, and the Australian Research Council's Project funding scheme under LP160101244. This work was also supported by National Natural Science Foundation of China No. 62101161.

communication devices such as sensors and monitors that are unable to transmit over a long distance due to the energy constraints [11]. Although the existing statistical MIMO channel models are suitable for most communication environment, the unique features, such as the three-dimensional (3D) space movement of UAVs at high altitude can not be captured [12]. Hence, recent work [12]–[15] proposed geometry-based UAV channel models for air-to-ground communication environment. The first work that considered the UAV's mobility from the moving velocities to directions in the vertical plane is reported in [12]. Moreover, authors in [13]–[15] derived the time-varying parameters of the angles of arrival (AoAs) and departure (AoDs) to describe the nonstationarity of the dynamic channel caused by the movement of the UAV. Differently, authors in [13] ignored the scatterers' movement and contained a LoS link and only one non-LoS link. Authors in [14] investigated the cluster-based multiple propagation paths. Besides, the initial azimuth and elevation AoAs and AoDs were further considered in [15].

Apart from UAVs aided communications that can provide effective communication services, the deployment of IRSs in wireless communications has attracted remarkable attention [16]. The IRS that consists of an array of reflecting elements with low cost and low energy consumption, can be installed in building facades, ceilings, indoor walls, road signs, as well as pedestrians' wearable devices [17]. By re-configuring the phase shifts of elements on the IRS, the reflected signals can be propagated. They can form virtual LoS links between mobile users and base stations with enhanced transmission signal power [18], [19]. Also, an IRS-aided system can improve spectral efficiency and enhance the communication coverage capability [20]. However, the promised communication performance brought by an IRS relies on good knowledge of CSI. Hence, obtaining accurate CSI with low complexity channel estimation and tracking approaches is indispensable and more challenging for practical IRS implementation [17].

Recently, channel estimation in IRS-assisted systems has been widely studied based on both conventional [21]–[25] and specific [26], [27] communication scenarios. For conventional scenarios, [21] proposed a three-phase pilot-based channel estimation framework for IRS-assisted MU communications, in which different links are estimated in different phases, separately. The authors in [22] developed two customized schemes, simultaneous-user channel estimation and sequential-user channel estimation, by separately considering different dominant links in the real-world scenario. Moreover, [23]–[25] all considered the conventional scenario but with part of the reflecting elements switched on in IRS. For some specific communication scenarios, [26] considered an indoor IRS-assisted channel model which assumed that the LoS path being blocked by the obstacles and the virtual LoS path reflected by IRSs as the major link. Double-IRS cooperatively aided MIMO system that has cascaded single-reflection and double-reflection links have been further exploited in [27].

Data-driven deep learning (DL) techniques have shown remarkable effectiveness to revolutionize communication systems [17]. In contrast to the traditional model driven channel estimation approaches, DL with powerful learning capabilities can be adopted for estimating the CSI that has beyond linear correlations in emerging advanced communication environment [28]–[32]. A deep residual learning method for channel estimation in IRS-assisted multi-user communications by considering the channel model with both LoS links and virtual LoS links is proposed in [28]. The authors in [29] proposed a learned denoising-based approximate message passing network to learn the channel structure for beamspace mmWave massive MIMO systems. Similarly, a deep denoising neural network-assisted CS channel estimation framework for IRS systems with reduced training overheads has been proposed in [30]. Moreover, authors of [31] developed a DL-based solution that enables IRS to learn to interact with the signal optimally. [32] proposed a twin convolutional neural network (CNN) architecture to estimate both LoS and cascaded non-LoS paths in IRS-assisted MIMO systems.

In the aforementioned work [21]–[32], the environment and the mobile users are assumed to be static for simplicity for channel estimation in an IRS-assisted communication system. However, in practice, the mobility of the environment cannot be ignored. Hence, time-varying channel estimation or channel tracking is a potential research topic but full of challenge. Furthermore, the proposed DL channel estimation techniques in [28]–[32] simply considered off-line training. None of the mentioned work considered the time-sequence of historical information for channel tracking.

B. Motivation and Contribution

Although UAVs can be flexibly adjusted to create a reliable communication environment by establishing LoS links and shortening the communication distances, it's inevitable that communication channels can still be occasionally blocked by obstacles, such as trees and high-rise buildings. The new technique called IRS-assisted UAV communication has been brought increasing attention [4], [33]–[35]. For example, [4] jointly designed the UAV trajectory and IRS beamforming to optimize the system average achievable rate. [33] investigated the fair secrecy energy efficiency in the system where mobile UAV relay equipped with an IRS. In [34], the IRS-assisted UAV relaying system is studied, where the IRS is employed on the building to assist the communication between the device and the UAV. Similarly, [35] considered the system that facilitates a UAV relay and an IRS. Then the UAV positioning, IRS passive beamforming were jointly optimized by minimizing the decoding error rate. However, all these mentioned works assume that the CSI is known in advance. Hence, it is crucial to design a reliable channel tracking scheme in IRS-assisted UAV communications systems. There are mainly three challenges to tackle: good estimation performance, the small pilot overheads, and the time-varying channel caused by the mobility of both UAV and mobile users.

Motivated by the aforementioned literature review, we propose a DL-based channel tracking algorithm in IRS-assisted UAV-enabled communication systems with lower training overheads and significantly improved tracking performance. The main contributions are summarized as follows:

- From our knowledge, this is the first work that develops a 3D geometry-based dynamic channel model in IRS-

assisted UAV-enabled communication system with fixed IRS, navigation UAV, and mobile users. We define the time-variant channel model consisting of both dynamic LoS link (user-UAV) with blockage parameter and dynamic cascaded virtual LoS link (user-IRS-UAV) with activation parameter. The velocities, the max Doppler effects, the propagation delays and the time delays are specially included in the system model.
- We propose a DL-based channel tracking mechanism to track the time-varying channel in the developed system. The proposed algorithm consists of two modules: channel pre-estimation and channel tracking. The pre-estimation is achieved by using a deep neural network (DNN) to perform off-line training on pre-collected training dataset. The tracking module is designed as a stacked bi-directional long short term memory (Stacked Bi-LSTM) that can track the CSI over a time-varying channel in a data-driven manner. The Stacked Bi-LSTM is constructed by a framework that involves a certain historical trace-back period in the time sequence and bidirectional structure over multiple stacked layers.
- In comparison with the benchmark algorithms, the proposed channel tracking algorithm requires less epochs for the convergence of the loss function during the off-line training phase. Moreover, simulations demonstrate that the proposed scheme (DNN followed by Stacked Bi-LSTM) shows better channel tracking performance with smaller pilot overheads than the benchmark algorithms, and it has comparable complexity.

This paper is structured as follows. The IRS-assisted UAV-enabled wireless communication system is introduced in Section II. In Section III, a DL-based channel tracking algorithm is proposed. Then, the proposed channel tracking performance over a time-variant channel is quantified in Section IV. Finally, conclusions are drawn in Section V.

Notation: Throughout the paper, we use the following common notation. The complex numbers are denoted by $\mathbb{C}$. The transpose and the conjugate transpose are denoted by $(\cdot)^{\mathrm{T}}$, $(\cdot)^{\mathrm{H}}$ respectively. $\boldsymbol{I}$ is the identity matrix. $\mathcal{CN}$ (mean, covariance) indicates a complex Gaussian random vector with defined mean and covariance. tr$(\cdot)$ indicates the trace of the matrix. $\boldsymbol{A}\otimes\boldsymbol{B}$ denotes the Kronecker product. $\boldsymbol{A}\oplus\boldsymbol{B}$ denotes the direct sum. $\mathbb{E}[\cdot]$ is used to denote expectation. $\|\cdot\|$ is the l_2 norm.

II. System Model

This paper considers the uplink IRS-assisted UAV-enabled multi-user system, which consists of M element antenna array equipped on UAV and N reflecting elements installed on IRS serving K users. The k^{th} user is assumed to be equipped with a single antenna. To enhance the quality of wireless communication services between UAV and mobile users, IRS is considered to be placed at the high-rise building to provide extended coverage and enables less movement of UAV [36], [37].

As shown in Fig. 1 (a), there are mainly two different kinds of links in the system: the user-UAV LoS link and the user-IRS-UAV virtual LoS link. The k^{th} user-UAV LoS link at time t is represented by $\boldsymbol{d}_k(t) \in \mathbb{C}^{M\times 1}$. The k^{th} user-IRS-UAV virtual LoS link at time t is consisted of two LoS sub-links: the user-IRS sub-link $\boldsymbol{u}_k(t) \in \mathbb{C}^{N\times 1}$ and the IRS-UAV sub-link $\boldsymbol{G}(t) \in \mathbb{C}^{M\times N}$. The illustration details of the dynamic 3D IRS-assisted channel model is presented in Fig. 1 (b). The moving speed of UAV and k^{th} user are represented by v_{U} and v_k.

The LoS link between k^{th} user and UAV at time t is $\boldsymbol{d}_k(t) = [d_{k,m}(t,\tau)]_{M\times 1}$ [13], [15] with

$$\begin{aligned} d_{k,m}(t,\tau) = \Omega_{k,m} e^{-j2\pi f_c \tau_{k,m}} \delta(\tau - \tau_{\mathrm{U},k,\mathrm{LoS}}) \\ e^{j2\pi f_k t[\cos(\alpha_{\mathrm{U},k}-\gamma_{k,\alpha})\cos\beta_{\mathrm{U},k}\cos\gamma_{k,\beta}+\sin\beta_{\mathrm{U},k}\sin\gamma_{k,\beta}]} \\ e^{j2\pi f_{\mathrm{U}} t[\cos(\alpha_{\mathrm{U},k}-\gamma_{\mathrm{U},\alpha})\cos\beta_{\mathrm{U},k}]}, \end{aligned} \tag{1}$$

where $\Omega_{k,m}$ is the attenuation factor between the m^{th} $(0 \leqslant m \leqslant m^{'} \leqslant M)$[1] antenna element on UAV and the single antenna on k^{th} user, f_c is the carrier frequency, $\tau_{k,m} = L_{k,m}/c$ is the propagation delay of the waves between the m^{th} antenna element on UAV and single antenna on k^{th} user at time t with $L_{k,m}$ as the distance between user and m^{th} antenna element, $\tau_{\mathrm{U},k,\mathrm{LoS}}$ is the time delay of this k^{th} user-UAV LoS link at time t, $f_{\mathrm{U}} = \frac{v_U}{\lambda}$ and $f_k = \frac{v_k}{\lambda}$ are the maximum Doppler frequency caused by the movement of both UAV and k^{th} user, $\alpha_{\mathrm{U},k}$ and $\beta_{\mathrm{U},k}$ are the azimuth and elevation angle between the k^{th} user and UAV, $\gamma_{\mathrm{U},\alpha}$ and $\gamma_{\mathrm{U},\beta}$ are the azimuth and elevation angle of the UAV's moving direction, $\gamma_{k,\alpha}$ is the azimuth angle of the k^{th} user's moving direction associate with the UAV location. The time delay of this LoS link is

$$\tau_{\mathrm{U},k,\mathrm{LoS}} = \frac{D_k}{c_0 \cos\beta_{\mathrm{U},k}}, \tag{2}$$

with D_k as the xy-plane antenna center distance between UAV and k^{th} user, c_0 as light speed.

Note that, for vitual LoS link, the main difference between $d_{k,m}(t,\tau)$ in (1) and each LoS sub-link is that the IRS is installed at a fixed place without moving at all i.e., $f_{\mathrm{S}} = 0$. Hence, the k^{th} user-IRS LoS sub-link at time t is $\boldsymbol{u}_k(t) = [u_{k,n}(t,\tau)]_{N\times 1}$ with

$$\begin{aligned} u_{k,n}(t,\tau) = \Omega_{k,n} e^{-j2\pi f_c \tau_{k,n}} \delta(\tau - \tau_{\mathrm{S},k,\mathrm{LoS}}) \\ e^{j2\pi f_k t[\cos(\alpha_{\mathrm{S},k}-\gamma_{k,\alpha})\cos\beta_{\mathrm{S},k}]}, \end{aligned} \tag{3}$$

where $\Omega_{k,n}$ is the attenuation factor between the n^{th} $(0 \leqslant n \leqslant n^{'} \leqslant N)$ reflecting element on IRS and the single antenna on k^{th} user, $\tau_{\mathrm{S},k,\mathrm{LoS}}$ is the time delay of this k^{th} user-IRS LoS sub-link at time t, $\alpha_{\mathrm{S},k}$ and $\beta_{\mathrm{S},k}$ are the relative azimuth and elevation direction between k^{th} user and IRS, $\gamma_{k,\alpha}$ is the azimuth angle of the k^{th} user's moving direction, $\tau_{k,n} = L_{k,n}/c$ is the propagation delay of the waves between the n^{th} antenna element on IRS and single antenna on k^{th} user at time t with $L_{k,n}$ as the distance between user and n^{th} element on IRS.

$$\begin{aligned} u_{k,n}(t,\tau) = \Omega_{k,n} e^{-j2\pi f_c \tau_{k,n}} \delta(\tau - \tau_{\mathrm{S},k,\mathrm{LoS}}) \\ e^{j2\pi f_k t[\cos(\alpha_{\mathrm{S},k}-\gamma_{k,\alpha})\cos\beta_{\mathrm{S},k}]}, \end{aligned} \tag{4}$$

[1]The reason of having the $m^{'th}$ element presented in the illustration Fig. 1 is to show the antenna flat angle ψ_{U}. Similar to the existence of the $n^{'th}$ reflection element on IRS, the physical flat angle is represented by ψ_{S}.

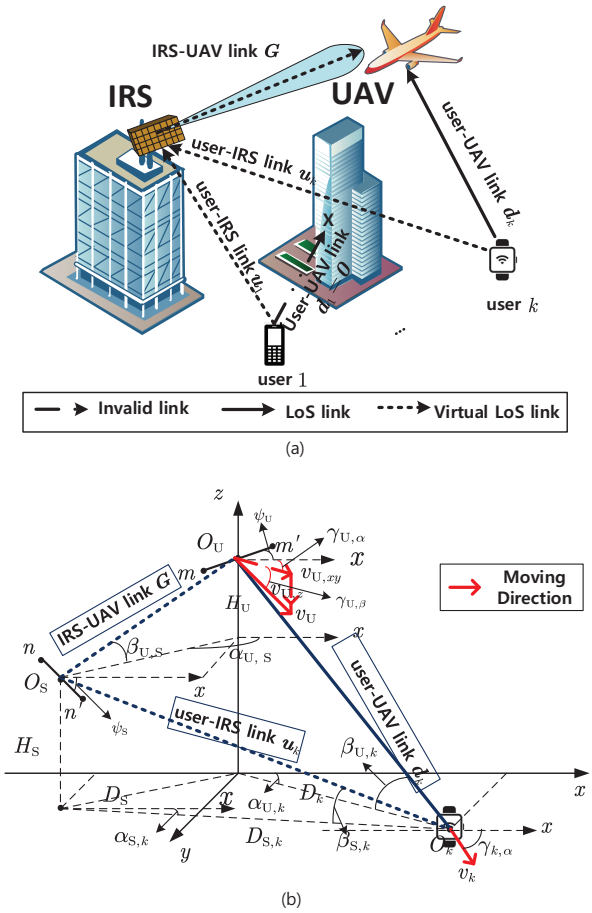

Fig. 1. (a) The illustration of the IRS-assisted UAV-enabled multi-user communication system. (b) The system model of the uplink of the IRS-assisted UAV-enabled multi-user communication.

where $\Omega_{k,n}$ is the attenuation factor between the n^{th} ($0 \leqslant n \leqslant n^{'} \leqslant N$) reflecting element on IRS and the single antenna on k^{th} user, $\tau_{\mathrm{S},k,\mathrm{LoS}}$ is the time delay of this k^{th} user-IRS LoS sub-link at time t, $\alpha_{\mathrm{S},k}$ and $\beta_{\mathrm{S},k}$ are the relative azimuth and elevation direction between k^{th} user and IRS, $\gamma_{k,\alpha}$ is the azimuth angle of the k^{th} user's moving direction, $\tau_{k,n} = L_{k,n}/c$ is the propagation delay of the waves between the n^{th} antenna element on IRS and single antenna on k^{th} user at time t with $L_{k,n}$ as the distance between user and n^{th} element on IRS.

The IRS-UAV LoS sub-link at time t is $\boldsymbol{G}_k(t) = [g_{m,n}(t,\tau)]_{M\times N}$ with

$$g_{m,n}(t,\tau) = \Omega_{m,n} e^{-j2\pi f_c \tau_{m,n}} \delta(\tau - \tau_{\mathrm{U,S,LoS}}) \\ e^{j2\pi f_{\mathrm{U}} t[\cos(\alpha_{\mathrm{U,S}}-\gamma_{\mathrm{U},\alpha})\cos\beta_{\mathrm{U,S}}\cos\gamma_{\mathrm{U},\beta}+\sin\beta_{\mathrm{U,S}}\sin\gamma_{\mathrm{U},\beta}]}, \quad (5)$$

where $\Omega_{m,n}$ is the attenuation factor between the m^{th} antenna element on UAV and the n^{th} reflecting element on IRS, $\tau_{\mathrm{U,S,LoS}}$ is the time delay of this IRS-UAV LoS sub-link at time t, $\alpha_{\mathrm{U,S}}$ and $\beta_{\mathrm{U,S}}$ are the relative azimuth and elevation direction between UAV and IRS, $\tau_{m,n} = L_{m,n}/c_0$ is the propagation delay of the waves between the m^{th} antenna element on UAV and n^{th} element on IRS with $L_{m,n}$ as the distance.

TABLE I
TABLE OF IMPORTANT SYMBOLS

Symbols	Explanations
$M, m, m^{'}$	Total number and index of antenna elements of UAV
$N, n, n^{'}$	Total number and index of elements of IRS
N_p	Total number of training pilot
$\alpha_{\mathrm{U},k}, \beta_{\mathrm{U},k}$	Azimuth and elevation AoAs/AoDs of user-UAV link
$\alpha_{\mathrm{S},k}, \beta_{\mathrm{S},k}$	Azimuth and elevation AoAs/AoDs of user-IRS link
$\alpha_{\mathrm{U,\,S}}, \beta_{\mathrm{U,\,S}}$	Azimuth and elevation AoA/AoD of IRS-UAV link
$\gamma_{\mathrm{U},\alpha}, \gamma_{\mathrm{U},\beta}$	Azimuth and elevation angle of UAV movement
$\gamma_{k,\alpha}$	Angle of k^{th} user movement
$\beta_{t,n}$	Amplitude at n^{th} element of IRS at time slot t
$\phi_{t,n}$	Phase shift at n^{th} element of IRS at time slot t
v_{U}	UAV movement speed
$v_{\mathrm{U},xy}, v_{\mathrm{U},z}$	UAV speed's horizontal and perpendicular components
v_k	Speed of k^{th} user movement
f_{U}	Maximum Doppler frequency of UAV
f_k	Maximum Doppler frequency of k^{th} user
ψ_{U}	Antenna physical flat angle on UAV
ψ_{S}	Reflection elements' physical flat angle on IRS
$\tau_{k,m}$	The propagation delay of the wave between UAV m^{th} antenna element and k^{th} user single antenna at time t
$\tau_{k,n}$	The propagation delay of the wave between IRS n^{th} reflection element and k^{th} user single antenna at time t
$\tau_{m,n}$	The propagation delay of the wave between UAV m^{th} antenna element and IRS n^{th} reflection element at time t
$\tau_{\mathrm{U},k,\mathrm{LoS}}$	The time delay of k^{th} user-UAV LoS link at time t
$\tau_{\mathrm{S},k,\mathrm{LoS}}$	The time delay of k^{th} user-IRS LoS link at time t
$\tau_{\mathrm{U,S,LoS}}$	The time delay of IRS-UAV LoS link at time t
D_k	The xy-plane center distance between UAV and k^{th} user
D_{S}	The xy-plane center distance between IRS and UAV
$D_{\mathrm{S,k}}$	The xy-plane center distance between IRS and k^{th} user
$\Omega_{k,m}$	Attenuation factor between the UAV m^{th} antenna element and the k^{th} user single antenna
$\Omega_{k,n}$	Attenuation factor between the IRS n^{th} reflection element and the k^{th} user single antenna
$\Omega_{m,n}$	Attenuation factor between the UAV m^{th} antenna element and the IRS n^{th} reflection element
$L_{k,m}$	The distance between the UAV m^{th} antenna element and the k^{th} user single antenna
$L_{k,n}$	The distance between the IRS n^{th} reflection element and the k^{th} user single antenna
$L_{m,n}$	The distance between the UAV m^{th} antenna element and the IRS n^{th} reflection element

The corresponding time delay for two sub-links at time t are

$$\tau_{\mathrm{S},k,\mathrm{LoS}} = \frac{D_{\mathrm{S},k}}{c_0 \cos\beta_{\mathrm{S},k}} \quad (6)$$

and

$$\tau_{\mathrm{U,S,LoS}} = \frac{D_{\mathrm{S}}}{c_0 \cos\beta_{\mathrm{U,S}}}. \quad (7)$$

The k^{th} user-IRS-UAV virtual LoS link at time t can be expressed as $\boldsymbol{G}(t)\boldsymbol{\Phi}(t)\boldsymbol{u}_k(t) \in \mathbb{C}^{M\times 1}$, in which $\boldsymbol{\Phi}(t) = \mathrm{diag}(\boldsymbol{\varphi}(t)) \in \mathbb{C}^{N\times N}$ is the phase shift matrix of IRS with $\boldsymbol{\varphi}(t) = [\beta_{t,1}e^{j\phi_{t,1}}, ..., \beta_{t,n}e^{j\phi_{t,n}}, ..., \beta_{t,N}e^{j\phi_{t,N}}]^T \in \mathbb{C}^{N\times 1}$, where $\beta_{t,n} \in [0,1]$ and $\phi_{t,n} \in [0, 2\pi]$ are the reflection amplitude and phase shift of the subsurface n of IRS at time slot t [26].

Hence, the IRS-assisted UAV uplink at time t is the superimposition of the vitual LoS link and the LoS link, which

can be given as

$$\begin{aligned}\dot{\boldsymbol{H}}_k(t) &= \boldsymbol{G}(t)\boldsymbol{\Phi}(t)\boldsymbol{u}_k(t) + \boldsymbol{\eta}_k\boldsymbol{d}_k(t) \\ &= \underbrace{\boldsymbol{G}(t)\text{diag}(\boldsymbol{u}_k(t))}_{\boldsymbol{H}_{\text{C},k}(t)}\boldsymbol{\varphi}(t) + \boldsymbol{\eta}_k\boldsymbol{d}_k(t), k = 1, ...K, \end{aligned} \quad (8)$$

where $\boldsymbol{H}_{\text{C},k}(t) \in \mathbb{C}^{M\times N}$ denotes the cascaded k^{th} user-IRS-UAV channel at time slot t, $\boldsymbol{\eta}_k \in \{0,1\}^{M\times 1}$ is the blockage parameter that is distributed according to a Bernoulli distribution [38] with the blockage probabilities for LoS link is p_k.

The received signal at the UAV from K users at time slot t can be expressed as

$$\begin{aligned}\boldsymbol{Y}(t)^{'} &= \sum_{k=1}^{K}\dot{\boldsymbol{H}}_k(t)\boldsymbol{s}_k + \boldsymbol{N}_k^{'}(t) \\ &= \sum_{k=1}^{K}\underbrace{[\boldsymbol{H}_{C,k}(t), \boldsymbol{\eta}_k\boldsymbol{d}_k(t)]}_{\boldsymbol{H}_k(t)}\underbrace{[\boldsymbol{\varphi}(t); 1]^T}_{\boldsymbol{r}(t)}\boldsymbol{s}_k + \boldsymbol{N}_k^{'}(t),\end{aligned} \quad (9)$$

where $\boldsymbol{Y}(t)^{'} \in \mathbb{C}^{M^{'}\times N_p}$ is the MU received signal, $\boldsymbol{H}_k(t) \in \mathbb{C}^{M\times(N+1)}$ is the channel matrix that need to be estimated, $\mathbf{r}(t) \in \mathbb{C}^{(N+1)\times 1}$, $\boldsymbol{s}_k \in \mathbb{C}^{1\times N_p}$ is the training pilot with $\boldsymbol{s}_k\boldsymbol{s}_k^H = \mathcal{P}N_p$ and $\boldsymbol{s}_{k_a}\boldsymbol{s}_{k_b} = 0$, where $\mathcal{P}$ is the power of each user, $k_a, k_b \in 1, 2, ..., K$, and $k_a \neq k_b$. $\boldsymbol{N}_k^{'}(t) \sim \mathcal{CN}(0, \sigma^2_{\boldsymbol{N}'}\boldsymbol{I})$ is the AWGN noise matrix.

For MU case, since the pilot sequences of each two users are orthogonal, the received signal vectors for k^{th} user can be decoupled by multiplying a sequence $\boldsymbol{s}_k^H$ as

$$\begin{aligned}\underbrace{\frac{1}{\mathcal{P}N_p}\boldsymbol{Y}(t)^{'}\boldsymbol{s}_k^H}_{\boldsymbol{Y}_k(t)} &= \dot{\boldsymbol{H}}_k(t) + \frac{1}{\mathcal{P}N_p}\boldsymbol{N}_k^{'}(t)\boldsymbol{s}_k^H \\ &= \underbrace{[\boldsymbol{H}_{C,k}(t), \boldsymbol{\eta}_k\boldsymbol{d}_k(t)]}_{\boldsymbol{H}_k(t)}\underbrace{[\boldsymbol{\varphi}(t); 1]^T}_{\boldsymbol{r}(t)} + \underbrace{\frac{1}{\mathcal{P}N_p}\boldsymbol{N}_k^{'}(t)\boldsymbol{s}_k^H}_{\boldsymbol{N}_k(t)},\end{aligned} \quad (10)$$

where $\boldsymbol{Y}_k(t) \in \mathbb{C}^{M\times N_p}$ is the received signal vector at the UAV from the k^{th} user, $\boldsymbol{H}_k(t) \in \mathbb{C}^{M\times(N+1)}$ is the channel matrix that need to be estimated, $\mathbf{r}(t) \in \mathbb{C}^{(N+1)\times 1}$, $\boldsymbol{N}_k(t) \sim \mathcal{CN}(0, \sigma^2_{\boldsymbol{N}}\boldsymbol{I})$.

The channel $\boldsymbol{H}_k(t)$ is estimated by a channel tracker, denoted by $\mathcal{F}(\cdot)$, which depends on the received signal $\boldsymbol{Y}_(t)^{'}$, $\boldsymbol{r}(t)$, and the training pilot $\boldsymbol{s}_k$. The estimated channel $\tilde{\boldsymbol{H}}_k(t) = \mathcal{F}(\boldsymbol{Y}_k(t); \boldsymbol{r}(t), \boldsymbol{s}_k)$. Hence, the pilot-aided channel estimation problem can be written as

$$\begin{aligned}\min_{\mathcal{F}} \mathbb{E}\left[\|\boldsymbol{H}_k(t) - \tilde{\boldsymbol{H}}_k(t)\|^2\right], \\ \text{s.t. } \text{tr}\left(\boldsymbol{s}_k\boldsymbol{s}_k^H\right) = E_s,\end{aligned} \quad (11)$$

where $E_s = N_pT_sP$ is the energy constraint with N_p as pilot overheads length, T_s as the length of one time slot, and P denotes the transmit power.

To be noticed, because of the mobility of both UAV and k^{th} user, the relative azimuth and elevation angle and the relative distance are constantly changing through time. We assume the initial position of the UAV is $(x_{\text{U}}, y_{\text{U}}, z_{\text{U}}) = (0, 0, H_{\text{U}})$, k^{th} user is $(x_k, y_k, z_k) = (D_k\cos\alpha_{\text{U},k}, D_k\sin\alpha_{\text{U},k}, 0)$, IRS is $(x_{\text{S}}, y_{\text{S}}, z_{\text{S}}) = (D_{\text{S}}\cos\alpha_{\text{U},k}, D_{\text{S}}\sin\alpha_{\text{U},k}, H_{\text{S}})$. The UAV speed v_{U} has the moving direction $\gamma_{\text{U},\alpha}$ and $\gamma_{\text{U},\beta}$. The user speed v_k has the moving direction $\gamma_{k,\alpha}$. Hence, the location should be updated for t^{th} time slot, i.e., UAV is $(0, 0, H_{\text{U}} - v_{\text{U}}t\sin\gamma_{\text{U},\beta})$, k^{th} user is $(D_k\cos\alpha_{\text{U},k} + v_kt\cos\gamma_{k,\alpha}, D_k\sin\alpha_{\text{U},k} + v_kt\sin\gamma_{k,\alpha}, 0)$. Hence, the updated relative azimuth, elevation angles and distances in (1)-(7) can be calculated based on new locations. Furthermore, we assumed that the antenna on UAV has fixed physical flat position angle ψ_{U}. Similarly, the reflecting surface on IRS has fixed physical flat position angle ψ_{S}. The element distance on both antenna and reflecting surface is $\Delta = \lambda/2$. Therefore, the propagation delay of the waves $\tau_{k,m}, \tau_{k,n}, \tau_{m.n}$ can be calculated accordingly.

By taking the relative position in Fig.1(b) as an example, with $\Delta_m = \frac{1}{2}(M + 1 - 2m)\Delta$ as the distance between m^{th} element and the center O_{U}, and $\Delta_n = \frac{1}{2}(N+1-2n)\Delta$ as the distance between n^{th} element and the center O_{S}, the distance between k^{th} user and m^{th} element on UAV antenna $L_{k,m}$, the distance between k^{th} user and n^{th} element on IRS is $L_{k,n}$, and the distance between m^{th} element on UAV antenna and n^{th} element on IRS is $L_{m,n}$ are calculated as in (12), (13), and (14).

III. Proposed Deep Learning Based Channel Tracking Algorithm

Data-driven DL based framework is now widely designed and employed for channel estimation [39]–[41]. This is because that DL can extract the characteristics of the complex environment information from received signals without the need of prior knowledge about the channel statistics [41]. Additionally, DL-based algorithms have low computational complexity with simple operations such as multiplications [40]. However, all these DL-based channel estimation work ignore the time sequence of the CSI. In another word, the adjacent observations of the time-varying CSI can be further utilized for more precise prediction.

To track the time varying channel, it is necessary to give neural networks the ability of learning the behavior of the correlation across time domain. There are two widely considered methods called recurrent neural network (RNN) and LSTM on solving the time-varying tasks, such as natural language processing. Both methods consider the information from the previously entered data and the currently entered data to predict. Specially, RNN has feedback loops to maintain information over time. However, it's difficult for RNN on learning long-term temporal dependencies due to the vanishing gradient problem. Differently, LSTM introduces input and forget gates for better preservation of long-term dependencies on dealing gradient flow [42].

By combining the advantages of DNN with multilayer perception mechanism on extracting characteristics of complex environment and LSTM with different input/output layers on passing information across time domain, in this section, DNN followed by Stacked Bi-LSTM framework is proposed to track the time sequence CSI in IRS-assisted UAV communication systems. The illustration of the overall structure

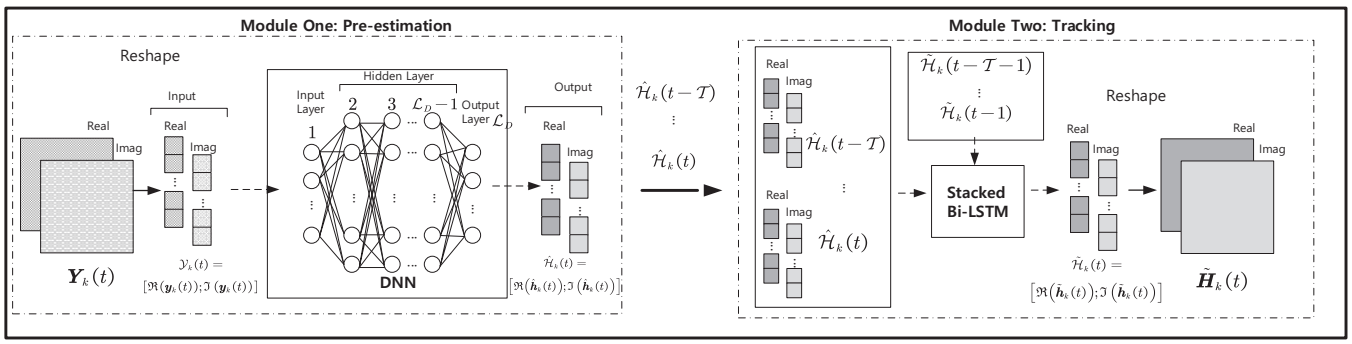

Fig. 2. The illustration framework of the overall channel tracking algorithm.

$$L_{k,m} = \sqrt{(|D_k \sin\alpha_{\mathrm{U},k}| - \Delta_m \sin\psi_{\mathrm{U}})^2 + (D_k \cos\alpha_{\mathrm{U},k} + \Delta_m \cos\psi_{\mathrm{U}})^2 + z_{\mathrm{U}}^2}, \tag{12}$$

$$L_{k,n} = \sqrt{(|D_{\mathrm{S},k} \sin\alpha_{\mathrm{S},k}| - \Delta_n \sin\psi_{\mathrm{S}})^2 + (D_{\mathrm{S},k} \cos\alpha_{\mathrm{S},k} + \Delta_n \cos\psi_{\mathrm{S}})^2 + z_{\mathrm{S}}^2}, \tag{13}$$

$$L_{m,n} = \sqrt{\begin{aligned}(|D_{\mathrm{S}} \cos\alpha_{\mathrm{U,S}}| - \Delta_m \cos\psi_{\mathrm{U}} + \Delta_n \cos\psi_{\mathrm{S}})^2 + (D_{\mathrm{S}} \sin\alpha_{\mathrm{U,S}} + \Delta_n \sin\psi_{\mathrm{S}} - \\ \Delta_m \sin\psi_{\mathrm{U}})^2 + (z_{\mathrm{U}} - z_{\mathrm{S}})^2\end{aligned}}. \tag{14}$$

of the proposed algorithm is shown in Fig. 2. There are mainly two modules in this framework: DNN for denoising pre-estimation based on off-line trained model and Stacked Bi-LSTM for tracking with assist of the history sequence information. To present the channel tracking problem in the vector form, we denote $\boldsymbol{y}_k(t) = \mathrm{vec}\left(\boldsymbol{Y}_k(t)\right) \in \mathbb{C}^{MN_p \times 1}$ and $\boldsymbol{h}_k(t) = \mathrm{vec}\left(\boldsymbol{H}_k(t)\right) \in \mathbb{C}^{M(N+1)\times 1}$.

A. Module One: DNN Channel Estimation Framework

DNN is an extension version of the artificial neural network with multiple hidden layers between the input and output layers [43]. To be specific, each hidden layer has multiple neurons and each output is the weighted sum of neurons operated by a nonlinear function. The Sigmoid function $f_{\text{Sigmoid}}(x) = \frac{1}{1+e^{-x}}$ and the ReLU functions $f_{\text{ReLU}}(x) = \max(0, x)$ are the widely used nonlinear function for activation in the DNN.

The pre-estimation DNN is shown in Fig. 2(a) with $\mathcal{L}_D - 2$ hidden layers among total $\mathcal{L}_D$ layers. The l^{th} hidden layer of the network consists of N_e neurons where $2 \leqslant l \leqslant \mathcal{L}_D - 1$ and $1 \leqslant n_e \leqslant N_e$. The DNN input vector $\mathcal{Y}_k(t) = [\Re(\boldsymbol{y}_k(t)); \Im(\boldsymbol{y}_k(t))] \in \mathbb{R}^{MN_P \times 2}$ with the real and imaginary part of $\boldsymbol{y}_k(t)$ as $\Re(\boldsymbol{y}_k(t)) = [\Re(y_{k,1}(t)), ..., \Re(y_{k,MN_p}(t))]$ and $\Im(\boldsymbol{y}_k(t)) = [\Im(y_{k,1}(t)), ..., \Im(y_{k,MN_p}(t))]$, respectively. The total number of input layer neurons is $2MN_p$. Similarly, the DNN output vector $\hat{\mathcal{H}}_k(t) = [\Re(\hat{\boldsymbol{h}}_k(t)); \Im(\hat{\boldsymbol{h}}_k(t))] \in \mathbb{R}^{M(N+1)\times 2}$. The total number of output layer neurons is $2M(N+1)$. The total number of neurons on each hidden layer is defined as $16MN_P$.

To express the DNN transmission principle, we use $\boldsymbol{i}_l$ represents the input of the l^{th} layer neurons. o_{l,n_e} represents the output of the n_e^{th} neuron at l^{th} layer. $\boldsymbol{W}_l^{(\text{DNN})}$ and $\boldsymbol{b}_l^{(\text{DNN})}$ denote the weight matrix and the bias vector of the l^{th} layer. Hence, each neuron's output can be expressed as

$$o_{l,n_e} = f_{l,n_e}\left(b_{l,n_e}^{(\text{DNN})} + \boldsymbol{w}_{l,n_e}^{(\text{DNN})T} \boldsymbol{i}_l\right), \tag{15}$$

with f_{l,n_e} as the activation function for l^{th} layer and n_e^{th} neuron. For training stage, with total $\mathcal{B}$ batch size, the output of the DNN with $\dot{b}^{th}$ batch can be expressed as

$$\hat{\mathcal{H}}_k(\dot{b}, t) = \boldsymbol{f}_{\mathcal{L}_D}(...\boldsymbol{f}_2(\mathcal{Y}_k(\dot{b}, t); \boldsymbol{\theta}_2)...; \boldsymbol{\theta}_{\mathcal{L}_D}). \tag{16}$$

During the training phase of constructing DNN, the parameter set $\boldsymbol{\theta}_l = (\boldsymbol{W}_l^{(\text{DNN})}, \boldsymbol{b}_l^{(\text{DNN})})$ which represents the weights and biases of the DNN model at the l^{th} layer can be obtained through gradient descent by recursively minimize the loss function $\text{Loss}(\boldsymbol{\theta})$ until convergence. The loss function across

Algorithm 1 Training of Module One: Channel Pre-estimation DNN

Input: Training received signal $\mathcal{Y}_k(1), ..., \mathcal{Y}_k(T)$, training true channel information $\mathcal{H}_k(1), ..., \mathcal{H}_k(T)$.

Output: Trained pre-estimation DNN.

Initialization: Randomize initial weights $\boldsymbol{\theta}$.

1: Generate a set of training sequences $\mathcal{Y}_k(1), ..., \mathcal{Y}_k(T)$ and $\mathcal{H}_k(1), ..., \mathcal{H}_k(T)$ with selected SNRs and pilot overheads size N_P.
2: Design the pre-estimation DNN framework with $\mathcal{L}_D$ layers and N_e neurons in each hidden layer. Set the learning rate and batch size.
3: **while** not convergence **do**
4: Update weights $\boldsymbol{\theta}$ by minimizing loss function in (17).
5: **end while**

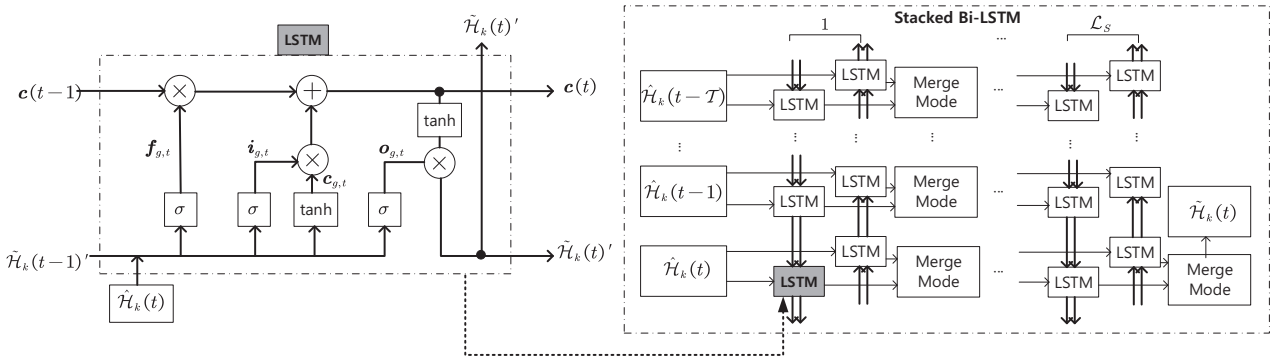

Fig. 3. The structure of Stacked Bi-LSTM.

all the layers is defined as

$$\text{Loss}(\boldsymbol{\theta}) = \frac{1}{2M(N+1)\mathcal{B}} \sum_{\dot{b}}^{\mathcal{B}} \left(\hat{\mathcal{H}}_k(\dot{b},t) - \mathcal{H}_k(\dot{b},t) \right)^2, \quad (17)$$

with $\boldsymbol{\theta}$ denotes all the parameter set across all the layers, $\mathcal{H}_k(\dot{b},t) = [\Re(\boldsymbol{h}_k(\dot{b},t)); \Im(\boldsymbol{h}_k(\dot{b},t))]$ denotes the true value of the channel in the $\dot{b}^{th}$ batch of the training process. The detail of the training process of the channel pre-estimation DNN can be found in **Algorithm 1**.

B. Module Two: Stacked Bi-LSTM Channel Tracking

As the second module of the overall algorithm framework, Stacked Bi-LSTM tracks the time sequence CSI based on pre-estimation denoised channel information (i.e., $\hat{\mathcal{H}}_k(t-\mathcal{T})$ to $\hat{\mathcal{H}}_k(t)$) and previous channel tracking output (i.e., $\tilde{\mathcal{H}}_k(t-\mathcal{T}-1)$ to $\tilde{\mathcal{H}}_k(t-1)$). Specifically, $\mathcal{T}$ denotes the total history time slot utilized in the model.

1) LSTM: As an enhancement of the recurrent neural network, LSTM is a gradient-based learning algorithm which is able to connect previous information to the current task [44], [45]. Normally, the time sequence data fed to the LSTMs along the chain-like structure in a forward direction. The illustration of a single LSTM cell is shown in Fig. 3 on the left hand side. (This illustration structure only takes the first layer forward LSTM as an example.)

The main difference between LSTM architecture and widely known recurrent neural networks (RNN) is the hidden layers in each LSTM cell. The first layer is called forget layer which is also known as the forget gate $\boldsymbol{f}_{g,t}$. It is consist of the information passed from previous layer $\mathcal{H}(t-1)$ and current denoised input $\hat{\mathcal{H}}(t)$ with weights $\tilde{\boldsymbol{W}}_f, \hat{\boldsymbol{W}}_f$ and bias $\boldsymbol{b}_f$ along with activation function:

$$\boldsymbol{f}_{g,t} = \sigma\left(\hat{\boldsymbol{W}}_f \hat{\mathcal{H}}_k(t) + \tilde{\boldsymbol{W}}_f \tilde{\mathcal{H}}_k(t-1) + \boldsymbol{b}_f \right). \quad (18)$$

The second layer is the input gate $\boldsymbol{i}_{g,t}$ which can be written as

$$\boldsymbol{i}_{g,t} = \sigma\left(\hat{\boldsymbol{W}}_i \hat{\mathcal{H}}_k(t) + \tilde{\boldsymbol{W}}_i \tilde{\mathcal{H}}_k(t-1) + \boldsymbol{b}_i \right). \quad (19)$$

It has the similar structure as the forget gate $\boldsymbol{f}_{g,t}$ but with different weights $\tilde{\boldsymbol{W}}_i, \hat{\boldsymbol{W}}_i$ and bias $\boldsymbol{b}_i$. The third layer is the cell input state $\boldsymbol{c}_{g,t}$ that can be calculated as

$$\boldsymbol{c}_{g,t} = \tanh\left(\hat{\boldsymbol{W}}_c \hat{\mathcal{H}}_k(t) + \tilde{\boldsymbol{W}}_c \tilde{\mathcal{H}}_k(t-1) + \boldsymbol{b}_c \right), \quad (20)$$

through a tanh function. The final layer is called output gate $\boldsymbol{o}_{g,t}$, which can be calculated as

$$\boldsymbol{o}_{g,t} = \sigma\left(\hat{\boldsymbol{W}}_o \hat{\mathcal{H}}_k(t) + \tilde{\boldsymbol{W}}_o \tilde{\mathcal{H}}_k(t-1) + \boldsymbol{b}_o \right). \quad (21)$$

To summarize the aforementioned hidden layers structure, $\boldsymbol{W}$ and $\boldsymbol{b}$ are the weight matrix and bias vector of the corresponding parameters. σ represents the gate activation function which is normally sigmoid function.

Apart from the cell input state $\boldsymbol{c}_{g,t}$ in the hidden layers, there are two other cell states in the structure: the previous cell output state $\boldsymbol{c}(t-1)$ fed in the current LSTM cell, and the current cell output state $\boldsymbol{c}(t)$ passed to the next LSTM cell. The output state at current time t can be updated as

$$\boldsymbol{c}(t) = \boldsymbol{f}_{g,t} \otimes \boldsymbol{c}(t-1) + \boldsymbol{i}_{g,t} \otimes \boldsymbol{c}_{g,t}. \quad (22)$$

More importantly, the conventional input layer is the denoised time sequence $\hat{\mathcal{H}}_k(t)$ at time slot t passed from DNN pre-estimation. Finally, the output layer can be calculated as

$$\tilde{\mathcal{H}}_k(t)' = \boldsymbol{o}_{g,t} \otimes \tanh(\boldsymbol{c}(t)). \quad (23)$$

2) Stacked Bi-LSTM: The illustration of the Stacked Bi-LSTM is shown in Fig. 3 on the right hand. To overcome the drawback of single LSTM cell which can only capture the history information, bidirectional structure has been proposed to combine both forward and backward directions to be able to utilize both history and future information [46]. Hence the forward output $\tilde{\mathcal{H}}_k(t)'^{(f)}$ and backward output $\tilde{\mathcal{H}}_k(t)'^{(b)}$ of each LSTM cell is calculated based on the relative input and the output layer function in (23). The forward layer output is iteratively calculated based on the time slot $t-\mathcal{T}$ to $t-1$. Similarly, the backward layer output is calculated based on the reversed time sequence $t-1$ to $t-\mathcal{T}$. The output of bidirectional structure can be expressed as

$$\tilde{\mathcal{H}}_k(t)' = \sigma_{f,b}\left(\tilde{\mathcal{H}}_k(t)'^{(f)} \oplus \tilde{\mathcal{H}}_k(t)'^{(b)} \right), \quad (24)$$

Algorithm 2 Training of Module Two: Channel Tracking Stacked Bi-LSTM

Input: Pre-estimation $\hat{\mathcal{H}}_k(1),...,\hat{\mathcal{H}}_k(T)$ training sequence, true channel information $\mathcal{H}_k(1),...,\mathcal{H}_k(T)$ training sequence.
Output: Trained tracking model for the current sequence.
Initialization: Randomize initial weights $\boldsymbol{W}$ and bias $\boldsymbol{b}$.

1: Generate a new set of training sequences $\hat{\mathcal{H}}_k(1),...,\hat{\mathcal{H}}_k(T)$ and $\mathcal{H}_k(1),...,\mathcal{H}_k(T)$ with selected SNR, pilot overheads size N_P, and $\mathcal{T}$ historic time step.
2: Design the bi-directional tracking framework with $\mathcal{L}_S$ stacked layers and $\mathcal{T}$ historic time step in each layer. Set the learning rate and batch size.
3: **while** not convergence **do**
4: Update weights $\boldsymbol{W}$ and bias $\boldsymbol{b}$ by minimizing loss function in (17).
5: **end while**

Algorithm 3 Proposed Overall Channel Tracking Algorithm

Input: Received signal $\mathcal{Y}_k(1),...,\mathcal{Y}_k(T)$.
Output: Channel tracking information $\tilde{\mathcal{H}}_k(T)$.

% Module One Channel Pre-estimation:
1: Construct the $\mathcal{L}_D$ layers DNN framework.
2: Load the DNN optimized parameters that has been trained in **Algorithm 1**.
3: Pre-estimate the channel information $\hat{\mathcal{H}}_k(1),...,\hat{\mathcal{H}}_k(T)$.
% Module Two Channel Tracking:
4: Train the channel tracking model as in **Algorithm 2** with $(T-1)$ sequence data and $\mathcal{T}$ historic time step.
5: Use time sequence $T-\mathcal{T}$ to $T-1$ as input data to track T channel information $\tilde{\mathcal{H}}_k(T)$ based on the trained tracking model.

which is the combination of the forward and backward output with the pre-defined merge mode $\sigma_{f,b}$. The $\sigma_{f,b}$ function can be concatenating, summation, average or multiplication.

It has been proved that by stacking multiple hierarchical models, the performance can be improved progressively [47]. Hence, we adopt a stacked structure where the output from the lower layer is then fed as the input to the upper layer with $\mathcal{L}_S \geqslant 2$ Bi-LSTM layers. The workflow of the Stacked Bi-LSTM considers both forward and backward directions and deeper structure with $\mathcal{T}$ time slots. The final tracking output after the $\mathcal{L}_S^{th}$ layer of the Stacked Bi-LSTM can be written as

$$\tilde{\mathcal{H}}_k(t) = \sigma_{f,b}\left(\tilde{\mathcal{H}}_k(t)_{\mathcal{L}_S}^{'(f)} \oplus \tilde{\mathcal{H}}_k(t)_{\mathcal{L}_S}^{'(b)}\right). \tag{25}$$

The training process of the channel tracking Stacked Bi-LSTM can be found in **Algorithm 2**. The proposed overall channel tracking algorithm can be found in **Algorithm 3**.

IV. Numerical Results

In this section, the training loss of various algorithms, the channel tracking performance and the complexity are evaluated. Based on the framework with two modules, we specially compare the channel tracking performance of DNN, DNN followed by LSTM, DNN followed by Bi-LSTM and DNN followed by Stacked Bi-LSTM. Specifically, DNN followed by Stacked Bi-LSTM is the proposed algorithm we mainly focused on evaluated. Basic parameters are set as follows: carrier frequency $f_c = 5.2$GHz, the UAV speed $v_{\mathrm{U}} = 5m/s$ with azimuth and elevation angle of UAV speed $\gamma_{\mathrm{U},\alpha} = \pi/6$ and $\gamma_{\mathrm{U},\beta} = \pi/6$. The k^{th} user speed $v_k = 5m/s$ with azimuth angle of user speed $\gamma_{k,\alpha} = \pi/24$. To prove the superiority tracking performance of our proposed scheme, in the simulation, we consider one moving user in the system. Total number of IRS reflection elements $N = 8$ and total number of antenna elements on the k^{th} UAV $M = 8$. The antenna angle on UAV is $\psi_{\mathrm{U}} = \pi/6$, the reflecting surface on IRS has fixed physical flat angle $\psi_{\mathrm{S}} = \pi/6$. The height of UAV $H_{\mathrm{U}} = 2000m$, the height of IRS $H_{\mathrm{S}} = 100m$. The initial relative position of the UAV, IRS, and the k^{th} user is shown in Fig.1 (b) with IRS location as $(-600m, -600m, 100m)$ and UAV location as $(500m, 600m)$. The total time sequence is 200 time slots[2] with train test split rate set as 0.8 for channel tracking performance evaluation. To be noticed, during the off-line learning, the adaptive moment (Adam) estimation optimizer is employed.

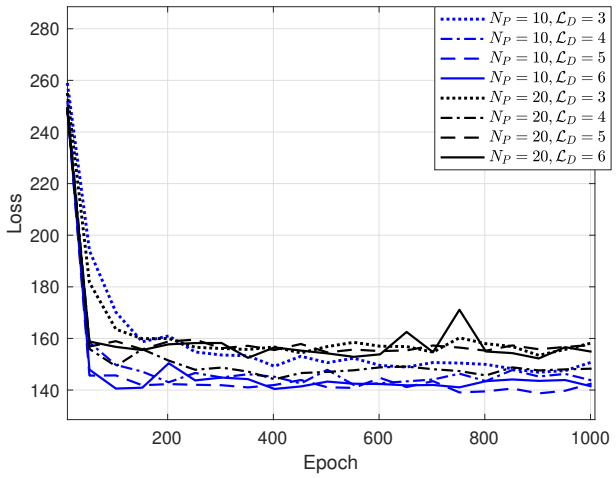

Fig. 4. Loss function of the channel pre-estimation DNN with different number of pilot overheads sizes $N_P = 10, 20$ and DNN total layers $\mathcal{L}_D = 3, 4, 5, 6$.

A. Loss function

Firstly, the loss function of the channel pre-estimation DNN with a different number of pilot overheads sizes N_P and hidden layers $\mathcal{L}_D$ are shown in Fig. 4. The total batch size $\mathcal{B}$ and learning rate ε are set as $512, 0.001$ for training the pre-estimation DNN. The total training data set is selected from many SNR$= -5, 0, 5, 10, 15, 20$dB and blockage probability from $p_k = 0.3, 0.4, 0.5, 0.6$ with $T = 200$ sequences. It can be observed that when $\mathcal{L}_D = 3$ for both $N_P = 10, 20$ require longer epochs to achieve convergence of the loss function. The difference for convergence of the loss function between $\mathcal{L}_D = 4, 5, 6$ is not significant. Besides, the converge loss for pilot overheads size $N_P = 10$ is lower than $N_P = 20$.

[2]For simplicity, we assume that the tracking signal is received in every time slot. This means that $T = 200$ in the simulation.

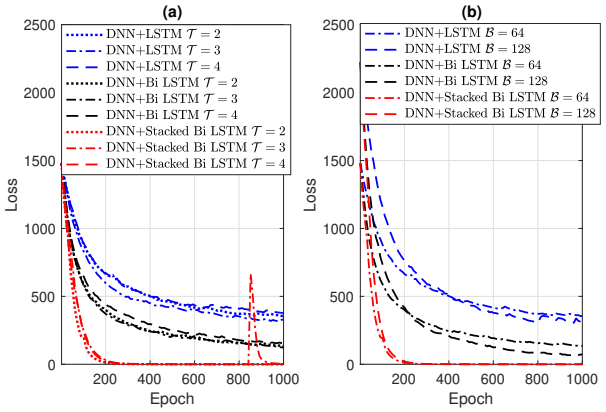

Fig. 5. (a) Loss function of various channel tracking methods with different historical time step $\mathcal{T}=2,3,4$. (b) Loss function of various channel tracking methods with different batch sizes $\mathcal{B}$.

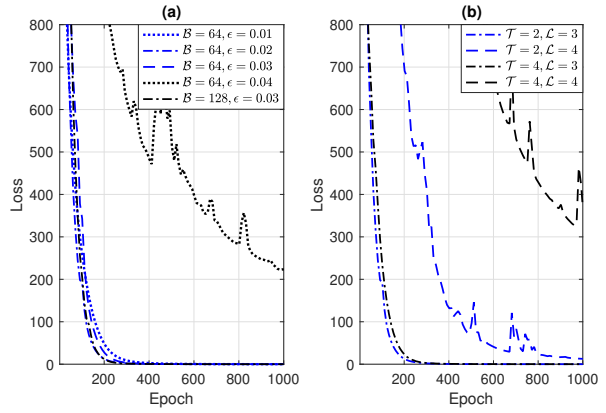

Fig. 6. (a) Loss function of the proposed algorithm with various batch sizes $\mathcal{B}$ and learning rate ϵ. (b) Loss function of the proposed algorithm with various historical time steps $\mathcal{T}=2,4$ and stacked layers $\mathcal{L}_S=3,4$.

The reason lies in that with N_P increases, the input size and neurons on each layer are increased accordingly, resulting in a more complex structure. Empirically, our model can achieve sufficient performance gain with relative small N_P. Hence, $\mathcal{L}_D=4$ and $N_P=10$ are adopted for the remaining simulations.

Secondly, the loss function of different channel tracking methods (LSTM, Bi-LSTM and proposed algorithm) are compared in Fig. 5. The proposed algorithm has total stacked layers $\mathcal{L}_S=3$. The channel sequence for training difference tracking methods is set as SNR$=$ 20dB and $p_k=0.3$ with a total $T=200$ sequence. In Fig.5 (a), different historical time step $\mathcal{T}=2,3,4$ are compared based on $\mathcal{B}=64$ and $\epsilon=0.02$. The proposed algorithm can quickly converge to loss near 0 for selected dynamic channel sequence epochs compared to the other two methods. It's worth noticing that the suitable hyper-parameter $\mathcal{T}$ can be selected differently based on various scenarios, such as different v_{U} and v_k. In Fig.5 (b), different batch size $64,128$ are compared based on $\mathcal{T}=2$ and $\epsilon=0.02$. The proposed algorithm shows a similar convergence performance.

Additionally, loss function of the proposed algorithm with different hyper-parameters are shown in Fig. 6 for the channel tracking of total $T=200$ dynamic channel under SNR$=$ 20dB, pilot overheads size $N_P=10$. By comparing different learning rates in Fig. 6 (a), $\mathcal{T}$ and $\mathcal{L}_S$ in Fig. 6 (b), $\epsilon=0.01$ with $\mathcal{B}=64$, $\mathcal{T}=2$ and $\mathcal{L}_S=3$, the hyper-parameter set that require slightly less epochs to achieve convergence of the loss function are selected for channel tracking performance evaluation in the following subsection.

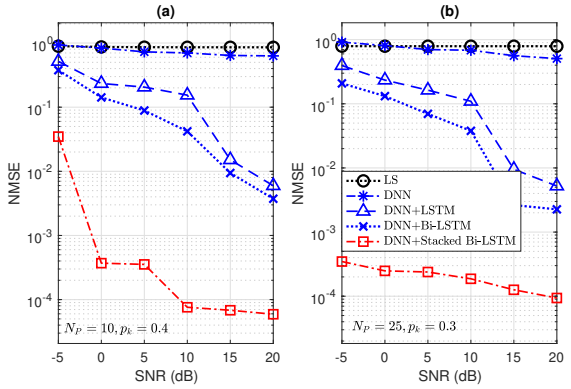

Fig. 7. NMSE performance for different algorithms.(a) $N_P=10$. (b)$N_P=25$.

B. Channel tracking performance

To evaluate the tracking performance of the algorithms, we refer the performance metric normalized mean square error (NMSE) [28] as

$$\mathrm{NMSE}=\frac{E\left(\|\tilde{\boldsymbol{H}}_k-\boldsymbol{H}_k\|^2\right)}{E\left(\|\boldsymbol{H}_k\|^2\right)}, \tag{26}$$

where $\tilde{\boldsymbol{H}}_k$ is the estimated tracking channel, $\boldsymbol{H}_k$ is the true channel. To evaluate the NMSE performance of the algorithms, the total $T=200$ sequence is divided into train and test data set with time slot $1-160$ as training set (for LSTM, Bi-LSTM and proposed) and $161-200$ as testing tracking data set. The performance is evaluated over the average of the total 500 rounds. A conventional least square (LS) algorithm [48] is applied in our system as a benchmark.

In Fig. 7, it can be observed that all algorithms show down trends NMSE performance with SNR increases. The proposed algorithm maintains significantly superior performance compared to other algorithms with small pilot overheads. It's worth noticed that LS and DNN are static estimation methods that only take the received signal into consideration for estimation. Differently, the rest three algorithms shows performance gain as they also observe the correlation across time domain. Specially, with bi-directional and stacked structure, our proposed algorithm can not only extract information from past, but also from future and deeper network structure.

C. Complexity

The complexity and computation time of different algorithms are characterize in this subsection. The complexity of the pre-estimation DNN without considering the bias is

TABLE II
TABLE OF OPERATION TIME (MILLISECOND) FOR CHANNEL PRE-ESTIMATION AND TRACKING

Module One: Different Layers of Pre-estimation DNN				
	$M=8, N=8$			$M=8, N=4$
	$N_P=10$	$N_P=15$	$N_P=20$	$N_P=10$
DNN $\mathcal{L}_D=3$	0.209	0.343	0.327	0.068
DNN $\mathcal{L}_D=4$	0.334	0.558	0.575	0.111
DNN $\mathcal{L}_D=5$	0.421	0.711	0.722	0.148
DNN $\mathcal{L}_D=6$	0.551	0.885	0.920	0.185
Module Two: Different Algorithms for Channel Tracking				
	$M=8, N=8$		$M=4, N=8$	
$N_P=10$	$\mathcal{T}=2$	$\mathcal{T}=5$	$\mathcal{T}=2$	$\mathcal{T}=5$
LSTM	2.956	2.983	0.283	0.394
Bi-LSTM	4.630	5.215	0.457	0.719
Stacked Bi-LSTM $\mathcal{L}_S=2$	8.770	10.543	0.733	1.442
Stacked Bi-LSTM $\mathcal{L}_S=3$	12.813	15.477	1.220	2.165

$\mathcal{O}\left(\sum_{l=1}^{\mathcal{L}_D-1}(N_e^l N_e^{l+1})\right)$ with N_e^l represents the neuron numbers in each layer. To be specific, the input layer ($l=1$) has $2MN_P$ neurons, each hidden layer ($l=2,...,(\mathcal{L}_D-1)$) has $16MN_P$ neurons, and the output layer ($l=\mathcal{L}_D$) has $2M(N+1)$ neurons. The complexity of a single LSTM cell can be calculated as $\mathcal{O}\left(N_c(4N_c+4N_i+N_o+3)\right)$ [49]. Specifically, N_c, N_i, N_o are the number of memory cell, the number of input units and the number of output units, respectively. The N_i and N_o are both $2M(N+1)$. Moreover, for LSTM $N_c=1\mathcal{T}$, Bi-LSTM $N_c=2\mathcal{T}$, Stacked Bi-LSTM $N_c=2\mathcal{T}\mathcal{L}_S$. For Bi-LSTM, the forward and backward bi-directional estimation gives $N_c=2\mathcal{T}$. For Stacked Bi-LSTM, with $\mathcal{L}_S$ multiple layers of Bi-LSTM stacked together, it's obvious that $N_c=2\mathcal{T}\mathcal{L}_S$.

As can be seen from Table. II that the Python Jupyter Notebook run-time of the multiple layers of pre-estimation DNN increases when layers $\mathcal{L}_D$, N_P, M increases. Besides, for channel tracking, Stacked Bi-LSTM requires a longer running time due to the complex structure, but achieves dramatically better NMSE performance over dynamic channel sequences, as proved in previous subsection.

V. CONCLUSION

In this paper, we developed the 3D geometry dynamic channel model in IRS-assisted UAV-enabled communication system. The navigation of UAV and the movement of mobile users are considered to construct the time-variant channel. There are mainly two dominant links in the channel model: dynamic LoS link (user-UAV) and dynamic virtual LoS link (user-IRS-UAV). We further proposed a novel DL-based channel tracking algorithm composed of two modules: DNN channel pre-estimation for denoising and Stacked Bi-LSTM for channel tracking. Specifically, Stacked Bi-LSTM is a framework that can trace historical information in the time sequence based on a bidirectional structure over multiple stacked layers. Simulation results have shown that the proposed channel tracking algorithm dramatically outperforms different benchmarks with small pilot overheads and comparable computation complexity.

REFERENCES

[1] Y. Zeng, R. Zhang, and T. J. Lim, "Wireless communications with unmanned aerial vehicles: opportunities and challenges," *IEEE Commun. Mag.*, vol. 54, no. 5, pp. 36–42, 2016.

[2] B. Li, Z. Fei, and Y. Zhang, "UAV communications for 5G and beyond: recent advances and future trends," *IEEE Internet Things J.*, vol. 6, no. 2, pp. 2241–2263, 2019.

[3] C. Zhang, W. Zhang, W. Wang, L. Yang, and W. Zhang, "Research challenges and opportunities of UAV millimeter-wave communications," *IEEE Wireless Communi.*, vol. 26, no. 1, pp. 58–62, 2019.

[4] S. Li, B. Duo, X. Yuan, Y.-C. Liang, and M. Di Renzo, "Reconfigurable intelligent surface assisted UAV communication: joint trajectory design and passive beamforming," *IEEE Wireless Commun. Lett.*, vol. 9, no. 5, pp. 716–720, 2020.

[5] M. A. ElMossallamy, H. Zhang, L. Song, K. G. Seddik, Z. Han, and G. Y. Li, "Reconfigurable intelligent surfaces for wireless communications: Principles, challenges, and opportunities," *IEEE Trans. Cogn. Commun. Netw.*, vol. 6, no. 3, pp. 990–1002, 2020.

[6] Q. Wu, S. Zhang, B. Zheng, C. You, and R. Zhang, "Intelligent reflecting surface aided wireless communications: A tutorial," *IEEE Trans. Commun.*, pp. 1–1, 2021.

[7] Z. Wei, Y. Cai, Z. Sun, D. W. K. Ng, J. Yuan, M. Zhou, and L. Sun, "Sum-rate maximization for IRS-assisted UAV OFDMA communication systems," *IEEE Trans. Wireless Commun.*, vol. 20, no. 4, pp. 2530–2550, 2021.

[8] Z. Mohamed and S. Aïssa, "Leveraging UAVs with intelligent reflecting surfaces for energy-efficient communications with cell-edge users," in *2020 IEEE International Conference on Communications Workshops (ICC Workshops)*, 2020, pp. 1–6.

[9] L. Ge, P. Dong, H. Zhang, J.-B. Wang, and X. You, "Joint beamforming and trajectory optimization for intelligent reflecting surfaces-assisted UAV communications," *IEEE Access*, vol. 8, pp. 78 702–78 712, 2020.

[10] X. Pang, M. Sheng, N. Zhao, J. Tang, D. Niyato, and K.-K. Wong, "When UAV meets IRS: Expanding air-ground networks via passive reflection," *IEEE Wireless Commun.*, vol. 28, no. 5, pp. 164–170, Nov 2021.

[11] M. Mozaffari, W. Saad, M. Bennis, and M. Debbah, "Mobile internet of things: Can uavs provide an energy-efficient mobile architecture?" in *2016 IEEE Global Communications Conference (GLOBECOM)*, 2016, pp. 1–6.

[12] H. Jiang, Z. Zhang, L. Wu, and J. Dang, "Three-dimensional geometry-based UAV-MIMO channel modeling for A2G communication environments," *IEEE Commun. Lett.*, vol. 22, no. 7, pp. 1438–1441, 2018.

[13] X. Cheng and Y. Li, "A 3-D geometry-based stochastic model for UAV-MIMO wideband nonstationary channels," *IEEE Internet Things J.*, vol. 6, no. 2, pp. 1654–1662, 2019.

[14] H. Jiang, Z. Zhang, and G. Gui, "Three-dimensional non-stationary wideband geometry-based UAV channel model for A2G communication environments," *IEEE Access*, vol. 7, pp. 26 116–26 122, 2019.

[15] H. Jiang, Z. Zhang, C. X. Wang, J. Zhang, J. Dang, L. Wu, and H. Zhang, "A novel 3D UAV channel model for A2G communication environments using AoD and AoA estimation algorithms," *IEEE Trans. Commun.*, vol. 68, no. 11, pp. 7232–7246, 2020.

[16] E. Basar, "Reconfigurable intelligent surface-based index modulation: A new beyond MIMO paradigm for 6G," *IEEE Trans. Commun.*, vol. 68, no. 5, pp. 3187–3196, 2020.

[17] Y. Liu, X. Liu, X. Mu, T. Hou, J. Xu, Z. Qin, M. Di Renzo, and N. Al-Dhahir, "Reconfigurable intelligent surfaces: Principles and opportunities," *arXiv preprint arXiv:2007.03435*, 2020.

[18] Z. Wang, Y. Shi, Y. Zhou, H. Zhou, and N. Zhang, "Wireless-powered over-the-air computation in intelligent reflecting surface-aided IoT networks," *IEEE Internet Things J.*, vol. 8, no. 3, pp. 1585–1598, 2021.

[19] C. Huang, R. Mo, and C. Yuen, "Reconfigurable intelligent surface assisted multiuser MISO systems exploiting deep reinforcement learning," *IEEE J. Sel. Areas in Commun.*, vol. 38, no. 8, pp. 1839–1850, 2020.

[20] G. Yu, X. Chen, C. Zhong, D. W. Kwan Ng, and Z. Zhang, "Design, analysis, and optimization of a large intelligent reflecting surface-aided B5G cellular internet of things," *IEEE Internet Things J.*, vol. 7, no. 9, pp. 8902–8916, 2020.

[21] Z. Wang, L. Liu, and S. Cui, "Channel estimation for intelligent reflecting surface assisted multiuser communications: Framework, algorithms, and analysis," *IEEE Trans. Wireless Commun.*, vol. 19, no. 10, pp. 6607–6620, 2020.

[22] B. Zheng, C. You, and R. Zhang, "Intelligent reflecting surface assisted multi-user OFDMA: channel estimation and training design," *IEEE Trans. Wireless Commun.*, vol. 19, no. 12, pp. 8315–8329, 2020.

[23] Y. Wang, H. Lu, and H. Sun, "Channel estimation in IRS-enhanced mmWave system with super-resolution network," *IEEE Commun. Lett.*, vol. 25, no. 8, pp. 2599–2603, 2021.

[24] X. Hu, R. Zhang, and C. Zhong, "Semi-passive elements assisted channel estimation for intelligent reflecting surface-aided communications," *IEEE Trans. Wireless Commun.*, pp. 1–1, 2021.

[25] C. You, B. Zheng, and R. Zhang, "Channel estimation and passive beamforming for intelligent reflecting surface: Discrete phase shift and progressive refinement," *IEEE J. Sel. Areas Commun.*, vol. 38, no. 11, pp. 2604–2620, 2020.

[26] X. Ma, Z. Chen, W. Chen, Z. Li, Y. Chi, C. Han, and S. Li, "Joint channel estimation and data rate maximization for intelligent reflecting surface assisted Terahertz MIMO communication systems," *IEEE Access*, vol. 8, pp. 99 565–99 581, 2020.

[27] B. Zheng, C. You, and R. Zhang, "Efficient channel estimation for double-IRS aided multi-user MIMO system," *IEEE Trans. Commun.*, pp. 1–1, 2021.

[28] C. Liu, X. Liu, D. W. K. Ng, and J. Yuan, "Deep residual learning for channel estimation in intelligent reflecting surface-assisted multi-user communications," *arXiv preprint arXiv:2009.01423*, 2020.

[29] Y. Zhang, Y. Mu, Y. Liu, T. Zhang, and Y. Qian, "Deep learning-based beamspace channel Estimation in mmWave massive MIMO systems," *IEEE Wireless Commun. Lett.*, vol. 9, no. 12, pp. 2212–2215, 2020.

[30] S. Liu, Z. Gao, J. Zhang, M. D. Renzo, and M. S. Alouini, "Deep denoising neural network assisted compressive channel estimation for mmWave intelligent reflecting surfaces," *IEEE Trans. Veh. Technol.*, vol. 69, no. 8, pp. 9223–9228, 2020.

[31] A. Taha, M. Alrabeiah, and A. Alkhateeb, "Enabling large intelligent surfaces with compressive sensing and deep learning," *IEEE Access*, pp. 1–1, 2021.

[32] A. M. Elbir, A. Papazafeiropoulos, P. Kourtessis, and S. Chatzinotas, "Deep channel learning for large intelligent surfaces aided mm-Wave massive MIMO systems," *IEEE Wireless Commun. Lett.*, vol. 9, no. 9, pp. 1447–1451, 2020.

[33] H. Long, M. Chen, Z. Yang, B. Wang, Z. Li, X. Yun, and M. Shikh-Bahaei, "Reflections in the sky: Joint trajectory and passive beamforming design for secure UAV networks with reconfigurable intelligent surface," *arXiv preprint arXiv:2005.10559*, 2020.

[34] L. Yang, F. Meng, J. Zhang, M. O. Hasna, and M. Di Renzo, "On the performance of RIS-assisted dual-hop UAV communication systems," *Trans. Veh. Technol.*, vol. 69, no. 9, pp. 10 385–10 390, Sep 2020.

[35] A. Ranjha and G. Kaddoum, "URLLC facilitated by mobile UAV relay and RIS: A joint design of passive beamforming, blocklength, and UAV positioning," *IEEE Internet Thing J.*, vol. 8, no. 6, pp. 4618–4627, Mar 2021.

[36] Q. Wu and R. Zhang, "Towards smart and reconfigurable environment: Intelligent reflecting surface aided wireless network," *IEEE Commun. Mag.*, vol. 58, no. 1, pp. 106–112, 2020.

[37] X. Liu, Y. Liu, and Y. Chen, "Machine learning empowered trajectory and passive beamforming design in UAV-RIS wireless networks," *arXiv preprint arXiv:2010.02749*, 2020.

[38] H. Iimori, G. T. F. de Abreu, O. Taghizadeh, R.-A. Stoica, T. Hara, and K. Ishibashi, "Stochastic learning robust beamforming for millimeter-wave systems with path blockage," *IEEE Wireless Commun. Lett.*, vol. 9, no. 9, pp. 1557–1561, 2020.

[39] H. Huang, J. Yang, H. Huang, Y. Song, and G. Gui, "Deep learning for super-resolution channel estimation and DOA estimation based massive MIMO system," *IEEE Trans. Veh. Technol.*, vol. 67, no. 9, pp. 8549–8560, 2018.

[40] A. K. Gizzini, M. Chafii, A. Nimr, and G. Fettweis, "Deep learning based channel estimation schemes for IEEE 802.11p standard," *IEEE Access*, vol. 8, pp. 113 751–113 765, 2020.

[41] Y. Yang, F. Gao, X. Ma, and S. Zhang, "Deep learning-based channel estimation for doubly selective fading channels," *IEEE Access*, vol. 7, pp. 36 579–36 589, 2019.

[42] J. Chung, C. Gulcehre, K. Cho, and Y. Bengio, "Empirical evaluation of gated recurrent neural networks on sequence modeling," *arXiv preprint arXiv:1412.3555*, 2014.

[43] J. Schmidhuber, "Deep learning in neural networks: An overview," *Neural networks*, vol. 61, pp. 85–117, 2015.

[44] S. Hochreiter and J. Schmidhuber, "Long short-term memory," *Neural computation*, vol. 9, no. 8, pp. 1735–1780, 1997.

[45] K. Greff, R. K. Srivastava, J. Koutník, B. R. Steunebrink, and J. Schmidhuber, "LSTM: a search space odyssey," *IEEE Transactions on Neural Networks and Learning Systems*, vol. 28, no. 10, pp. 2222–2232, 2017.

[46] M. Schuster and K. K. Paliwal, "Bidirectional recurrent neural networks," *IEEE Trans. Signal Process.*, vol. 45, no. 11, pp. 2673–2681, 1997.

[47] Y. Bengio, *Learning deep architectures for AI*. Now Publishers Inc, 2009.

[48] T. L. Jensen and E. De Carvalho, "An optimal channel estimation scheme for intelligent reflecting surfaces based on a minimum variance unbiased estimator," in *ICASSP 2020 - 2020 IEEE International Conference on Acoustics, Speech and Signal Processing (ICASSP)*, 2020, pp. 5000–5004.

[49] H. Sak, A. Senior, and F. Beaufays, "Long short-term memory based recurrent neural network architectures for large vocabulary speech recognition," *arXiv preprint arXiv:1402.1128*, 2014.

Jiadong Yu (S'18-M'22) received the PhD degree from Queen Mary University of London, U.K. in 2021. She was a teaching fellow in Queen Mary University of London in 2021. Since Nov. 2021, she has been with Internet of Things Thrust, the Hong Kong University of Science and Technology, Guangzhou, where she is currently a postdoctoral fellow. Her current research interests include the machine learning, deep learning, and federated learning for internet of things and wireless communications.

Xiaolan Liu (S'17-M'22) received the PhD degree from Queen Mary University of London, U.K. in 2021. She was a research assistant in King's College London from 2020-2021. Since Oct. 2021, she has been with the Institute for Digital Technologies, Loughborough University London, U.K., where she is currently a lecturer. Her current research interests include wireless distributed learning, multi-agent reinforcement learning for edge computing and machine learning for wireless communication optimization.

Yue Gao (S'03–M'07–SM'13) Yue Gao is a Professor at School of Computer Science, Fudan University, China. He received the Ph.D. degree from the Queen Mary University of London (QMUL), U.K., in 2007. He has then worked as a Lecturer, Senior Lecturer, Reader, and Chair Professor at QMUL and University of Surrey, respectively. His research interests include smart antennas, signal processing, intelligent network and computing in mobile, satellite and Internet of Things systems. He has published over 200 peer-reviewed journal and conference papers, 1 book and 5 book chapters and 3 best paper awards. He was a co-recipient of the EU Horizon Prize Award on Collaborative Spectrum Sharing in 2016 and elected as an Engineering and Physical Sciences Research Council Fellow in 2017. He is a member of the Board of Governors and Distinguished Lecturer of the IEEE Vehicular Technology Society (VTS), Vice-Chair of the IEEE ComSoc Wireless Communication Technical Committee, past Chair of the IEEE ComSoc Technical Committee on Cognitive Networks. He has been an Editor of several IEEE Transactions and Journals, and Symposia Chair, Track Chair, and other roles in the organising committee of several IEEE ComSoC, VTS and other conferences.

Chiya Zhang (S'15-M'19) received his Ph.D. degree in telecommunication engineering from the University of New South Wales, Sydney, Australia, in 2019. He is currently an Assistant Professor at Harbin Institute of Technology, Shenzhen, China. His current research interest is AI applications in telecommunication engineering. He received the Exemplary Reviewer Certificates of the IEEE Wireless Communications Letters in 2018 and IEEE ComSoc Asia-Pacific Outstanding Paper Award in 2020. He is currently serving as an Associate Editor for the IEEE Internet of Things Journal.

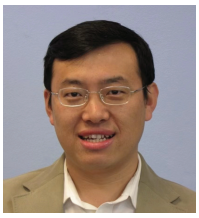

Wei Zhang (S'01-M'06-SM'11-F'15) received the Ph.D. degree from The Chinese University of Hong Kong in 2005. Currently, he is a Professor at the School of Electrical Engineering and Telecommunications, the University of New South Wales, Sydney, Australia. His current research interests include UAV communications, 5G and beyond. He received 6 best paper awards from IEEE conferences and ComSoc technical committees. He was elevated to Fellow of the IEEE in 2015 and was an IEEE ComSoc Distinguished Lecturer in 2016-2017. He is Vice President of IEEE Communications Society.

Within the IEEE ComSoc, he has taken many leadership positions including Member-at-Large on the Board of Governors (2018-2020), Chair of Wireless Communications Technical Committee (2019-2020), Vice Director of Asia Pacific Board (2016-2021), Editor-in-Chief of IEEE Wireless Communications Letters (2016-2019), Technical Program Committee Chair of APCC 2017 and ICCC 2019, Award Committee Chair of Asia Pacific Board and Award Committee Chair of Technical Committee on Cognitive Networks.

In addition, he has served as a member in various ComSoc boards/standing committees, including Journals Board, Technical Committee Recertification Committee, Finance Standing Committee, Information Technology Committee, Steering Committee of IEEE Transactions on Green Communications and Networking and Steering Committee of IEEE Networking Letters. Currently, he serves as an Area Editor of the IEEE Transactions on Wireless Communications and the Editor-in-Chief of Journal of Communications and Information Networks. Previously, he served as Editor of IEEE Transactions on Communications, IEEE Transactions on Wireless Communications, IEEE Transactions on Cognitive Communications and Networking, and IEEE Journal on Selected Areas in Communications – Cognitive Radio Series.